ADVANCED MATERIALS

www.advmat.de

Chloride Passivation of ZnO Electrodes Improves Charge Extraction in Colloidal Quantum Dot Photovoltaics

Jongmin Choi, Younghoon Kim, Jea Woong Jo, Junghwan Kim, Bin Sun, Grant Walters, F. Pelayo García de Arquer, Rafael Quintero-Bermudez, Yiying Li, Chih Shan Tan, Li Na Quan, Andrew Pak Tao Kam, Sjoerd Hoogland, Zhenghong Lu, Oleksandr Voznyy, and Edward H. Sargent**

The tunable bandgap of colloidal quantum dots (CQDs) makes them an attractive material for photovoltaics (PV). The best present-day CQD PV devices employ zinc oxide (ZnO) as an electron transport layer; however, it is found herein that ZnO's surface defect sites and unfavorable electrical band alignment prevent devices from realizing their full potential. Here, chloride (Cl)-passivated ZnO generated from a solution of presynthesized ZnO nanoparticles treated using an organic-solvent-soluble Cl salt is reported. These new ZnO electrodes exhibit decreased surface trap densities and a favorable electronic band alignment, improving charge extraction from the CQD layer and achieving the best-cell power conversion efficiency (PCE) of 11.6% and an average PCE of 11.4 ± 0.2%.

Colloidal quantum dots (CQDs) are promising semiconductors for optoelectronic devices, including light-emitting diodes,[1–3] photodetectors,[4,5] and photovoltaics[6–12] because of their size-dependent bandgap tunability, solution processability, and—when the surface is suitably treated to maintain the needed passivation under operating ambient conditions—their good air stability.[13–15] The performance of CQD photovoltaics (CQD-PVs) has been mainly improved through developments in device architectures[16–19] and surface passivation of the CQDs.[20,21] Recently, PbS inks with lead halide passivation yielded a certified power conversion efficiency (PCE) of 11.28%,[22] and a remaining further priority for the field of CQD photovoltaics is to identify heavy-metal-free colloidal nanomaterials that can provided the bandgap and performance needed for solar energy harvesting.

Dr. J. Choi, Dr. Y. Kim, Dr. J. W. Jo, Dr. J. Kim, Dr. B. Sun, G. Walters, Dr. F. P. García de Arquer, R. Quintero-Bermudez, Dr. C. S. Tan, Dr. L. N. Quan, A. P. T. Kam, Dr. S. Hoogland, Dr. O. Voznyy, Prof. E. H. Sargent
Department of Electrical and Computer Engineering
University of Toronto
10 King's College Road, Toronto, Ontario M5S 3G4, Canada
E-mail: o.voznyy@utoronto.ca; ted.sargent@utoronto.ca
Y. Li, Prof. Z. Lu
Department of Materials Science and Engineering
University of Toronto
184 College Street, Toronto, Ontario M5S 3E4, Canada

DOI: 10.1002/adma.201702350

The architecture used in CQD devices relies on a planar heterojunction between the CQD absorber layer and a wider bandgap electrode, which establishes a depletion region in the CQD layer for efficient charge separation and charge transport.[9,22] This depleted heterojunction is typically a rectifying junction between an n-type metal oxide semiconductor (e.g., TiO_2, ZnO, etc.) and a p-type CQD absorber layer.[23,24] Intensive attention has been dedicated to developing an efficient ZnO-based electron transport layer to improve device performance. Sol–gel-derived ZnO films are often employed and can feature different nanostructures,[25,26] interface engineering strategies,[8,27] and dopants.[28,29] Recent certified record PCEs have been achieved using spin-coated ZnO nanoparticles[9,22] that exhibited several advantages over sol–gel-derived ZnO films, such as improved conductivity due to larger grain size,[9,30,31] improved thickness control, and film formation without additional heat treatment (sol–gel-derived ZnO requires 200 °C annealing),[8,28] and suitability for mass-production and printable devices. Recently, Jang and co-workers explicitly compared the device performance of CQD PV devices employing ZnO nanoparticles and sol–gel-derived ZnO films, while using the same device configuration, and demonstrated the superiority of ZnO nanoparticles.[27]

Despite impressive progress from using ZnO electron transport layers, several characteristics of ZnO nanoparticles stand to be improved further.[32,33] ZnO nanoparticles possess high surface-to-volume ratios and so numerous surface defects, and these can act as electron trapping and charge recombination sites.[32] In addition, the conduction band (CB) level of ZnO nanoparticles (≈4.1 eV)[33] is not sufficiently deep to align well with the CB of PbS CQD films treated with iodide ligands (≈4.4 eV).[34] This discrepancy increases the rate of interfacial recombination due to inefficient charge extraction.[35–37] The development of better-passivated ZnO nanoparticles with a favorable band alignment offers therefore to provide a notable increase in CQD PV device performance.

Several approaches have been developed to reduce the surface defect density in ZnO, such as using interlayers, and organic and inorganic passivating agents.[8,27–29,32,38–41] The interlayer strategies, including self-assembled monolayers[8,39]

and conjugated polymers[27] introduced on top of ZnO films, prevent the direct contact between the electron transport layers and the CQD layer and form an interfacial dipole that favors electron extraction.[8,39] This approach, however, does not directly address the ZnO surface passivation problem. Incorporation of organic polymers, including poly(ethylene glycol) and poly(ethylene oxide),[30,40] aims to improve ZnO surface passivation but tends to hamper charge transport.[41] Reported inorganic passivating agents typically require heat treatment[28,29,38] and result in an upward shift of the CB[26,27,38] which leads to even poorer band alignment for electron extraction from the active layer.[35,37] It remains a key challenge to achieve—simultaneously—the strong passivation of ZnO nanoparticle surfaces and a favorable band alignment with the CQD layer in order to achieve efficient charge extraction.

To address these issues, we developed well-passivated ZnO nanoparticles that exhibit favorable band alignment for electron extraction in CQD-PV by a simple chloride (Cl)-passivation method, improving the CQD PV power conversion from 10.6% (10.4 ± 0.2%) to 11.6% (11.4 ± 0.2%).

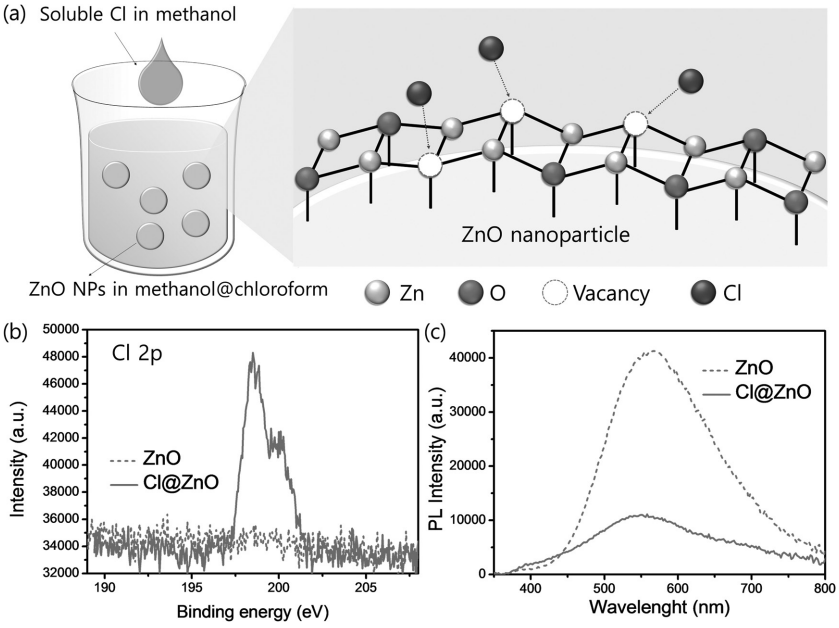

Figure 1. Surface passivation of ZnO nanoparticles by Cl. a) Schematic illustration of the Cl-passivation mechanism of ZnO (Cl@ZnO) nanoparticles by elimination of oxygen vacancies. b) Cl 2p X-ray photoelectron spectroscopy (XPS) spectra of ZnO and Cl@ZnO films deposited on glass. c) PL spectra of ZnO and Cl@ZnO films on glass.

The surface defect sites of ZnO are mainly derived from oxygen vacancies:[42] these have been reported to be capable of being filled with the aid of Cl passivation, as demonstrated for the case of ZnO nanowires.[43,44] Considering that bulky polymers can passivate the oxygen vacancies with simple solution mixing methods,[30,40] we expected that effective passivation can be achieved with soluble Cl salts. Concomitantly, the resulting films would possess a deeper conduction band due to the strong electronegativity and electron-withdrawing capability of the halides, in a process similar to that responsible for changes of the electron affinity in CQD films.[34] The Cl-passivated ZnO (Cl@ZnO) is achieved by adding a dissolved Cl salt in methanol into as-prepared ZnO nanoparticles dispersed in methanol-in-chloroform as shown in **Figure 1**a. The Cl@ZnO film deposited on indium tin oxide (ITO) glass exhibited very similar transmittance, film morphology, and nanoparticles size compared to those of ZnO electrode as shown in Figure S1 (Supporting Information). To investigate the binding affinity of Cl to ZnO nanoparticles, we employed X-ray photoelectron spectroscopy (XPS). The Cl 2p spectra of the ZnO layer shown in Figure 1b demonstrate the incorporation of Cl into Cl-treated ZnO. Furthermore, the slight peak shift of Zn 2p spectra for Cl@ZnO toward a higher binding energy compared to that of ZnO (from 1021.4 to 1021.7 eV as shown in Figure S2 in the Supporting Information) indicates that Cl is bound directly to Zn, considering that reported binding energies of Zn-O and Zn-Cl are 1021.4 and 1021.9 eV, respectively.[45,46] With X-ray photoelectron spectroscopy, we identified a ratio of Cl to Zn of 0.07. The photoluminescence (PL) analysis is a useful tool to investigate the surface defect density of ZnO films, and it is well known that the broad luminescence of ZnO films in the visible range (peaking near 550 nm) is derived from the defect sites of ZnO.[27,42] The decreased visible luminescence of Cl@ZnO films shown in Figure 1c reveals the reduction of the surface trap density due to Cl-passivation.

To assess the electronic energy band alignment of Cl@ZnO, we acquired Tauc plots and ultraviolet photoelectron spectra (UPS). The Tauc plots of ZnO layers (**Figure 2**a) indicate identical optical bandgaps before and after Cl-passivation (3.52 eV), which is similar to what is found for previously reported Cl-doped ZnO nanowires.[44] UPS spectra of ZnO layers in the low binding energy region (Figure 2b) show an upward shift (from 3.02 to 3.30 eV) of the Fermi level (E_F). Since the bandgaps of ZnO and Cl@ZnO are the same, the E_F rise must be due to increase the n-type doping in Cl@ZnO, a signature of trap filling.[47] Figure 2c shows the band alignment diagram of ZnO and Cl@ZnO deduced from the optical bandgaps (Figure 2a) and the UPS results (Figure 2b and Figure S3 (Supporting Information)). Deeper CB and valence band are obtained upon Cl-passivation, similar to observations in Cl-passivated TiO_2.[48] The deep electron affinity of Cl@ZnO is beneficial for electron extraction from CQD layer. In addition, the upward shift of E_F in Cl@ZnO can lead increased the V_{OC} and the depletion region width in the device.[17,28]

The advantages of the Cl@ZnO over conventional ZnO are seen in a comparison of CQD-PV devices. The device configuration of CQD PV is ITO/Cl@ZnO/PbS/PbS–1,2-ethanedithiol (EDT)/Au, where PbS layer is main light absorbing CQD layer and PbS–EDT layer acts as a hole transport layer (Figure S4, Supporting Information). The optimized Cl concentration of Cl@ZnO and thickness of the CQD layer are summarized in Figure S5 and Table S1 (Supporting Information). The PCE of Cl@ZnO-based devices saturated when the thickness of the

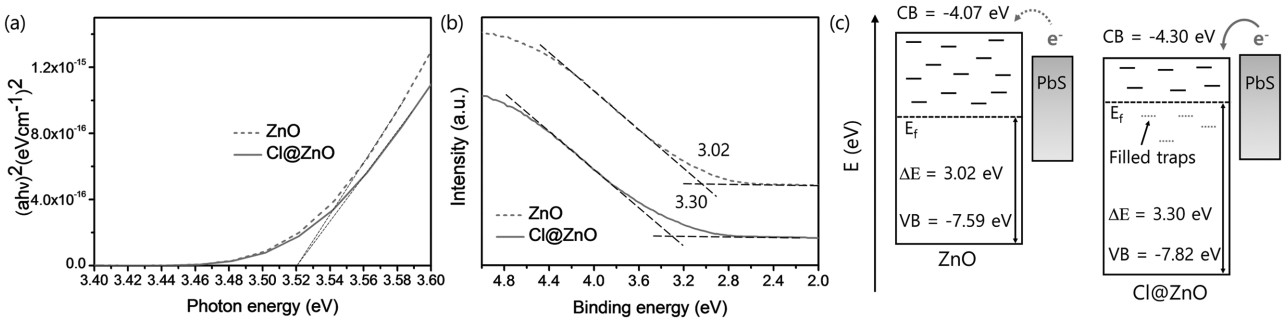

Figure 2. Electronic energy level alignment of Cl@ZnO. a) Tauc plots of ZnO and Cl@ZnO film on glass. b) Onset region of UPS spectra for each ZnO layer deposited on Au substrates (obtained from full UPS spectra shown in Figure S2 in the Supporting Information). c) Schematic band alignment diagram of ZnO and Cl@ZnO determined from optical bandgap and UPS analysis.

CQD layer reached 400 ± 10 nm (**Figure 3**a), using a 34×10^{-3} M concentration of Cl salt. The increased optimized CQD thickness (400 ± 10 nm) in the Cl@ZnO-based device compared to that (350 ± 10 nm)[22] of ZnO-based device might be due to a more favorable electrical band alignment and the resulting enhanced electron extraction of Cl@ZnO. The best-performing device with Cl@ZnO exhibited a superior PCE of 11.6% (an average PCE of 11.4 ± 0.2% with a V_{OC} of 0.63 ± 0.1 V, a J_{SC} of 27.8 ± 0.6 mA cm^{-2}, and a fill factor (FF) of 65.3 ± 1.7%) compared to 10.6% (an average PCE of 10.4 ± 0.2% with a V_{OC} of 0.61 ± 0.2 V, a J_{SC} of 26.9 ± 0.6% mA cm^{-2}, and a FF of 63.3 ± 2.3%) for a device with conventional ZnO (Figure 3b and Figure S6a (Supporting Information)) with reduced leakage current (Figure S6b, Supporting Information). The ZnO- and Cl@ZnO-based devices retain 95% of their initial PCE following 350 h of storage in air (Figure S6d, Supporting Information). The J_{SC} values obtained from each device agree well with the expected J_{SC} values measured from external quantum efficiency (EQE) spectra as shown in Figure S7 (Supporting Information) (ZnO- and Cl@ZnO-based devices are measured to be 27.5 and 28.9 mA cm^{-2}, respectively). All PV parameters were improved after Cl@ZnO was incorporated as the electron transport layer (Figure S6 and S8 and Table S2, Supporting Information). The increase in V_{OC} is induced by the upward shift of E_F in Cl@ZnO (Figure 2b,c). Meanwhile, the reason for the enhanced J_{SC} and FF in Cl@ZnO-based devices is the enhanced charge extraction ability of Cl@ZnO demonstrated by internal quantum efficiency (IQE) measurements. The IQE spectra (Figure 3c, obtained from Figure S7 and S9 in the Supporting Information) reveal the superior electron extraction ability of Cl@ZnO compared to conventional ZnO, mostly due to a wider depletion region width in the Cl@ZnO devices (Figure S10, Supporting Information). The *J–V* curves at negative bias (Figure 3b) reveal that the conventional ZnO device is not fully depleted even under J_{SC} conditions, suggesting insufficient doping of ZnO. At negative bias, both devices reach the same saturation current density, consistent with notion that they are identical thickness. Similarly, at the maximum power point, the depletion region width is improved from 210 nm in the ZnO control to 254 nm in the Cl@ZnO device, as assessed by capacitance–voltage analysis (Figure S10, Supporting Information).

In summary, we achieved an enhancement in CQD-PV performance via interfacial engineering of ZnO nanoparticles using solution-processed Cl passivation. In addition, the Cl@ZnO films exhibited beneficial electrical characteristics, including a deeper CB level and an upward shift of the E_F compared to conventional ZnO, and these favor efficient electron extraction. With these benefits, the CQD-PV devices based on Cl@ZnO showed a significant increase of PCE (11.4 ± 0.2%), compared to that of conventional ZnO-based device (10.4 ± 0.2%). Considering the versatile applicability of ZnO, the interfacial engineering method has the potential for further applications in photovoltaic, optoelectronic, and flexible devices.

Experimental Section

Preparation of Cl@ZnO Nanoparticles: The solution of ZnO nanoparticles were synthesized following a reported method.[22] The NaCl solution

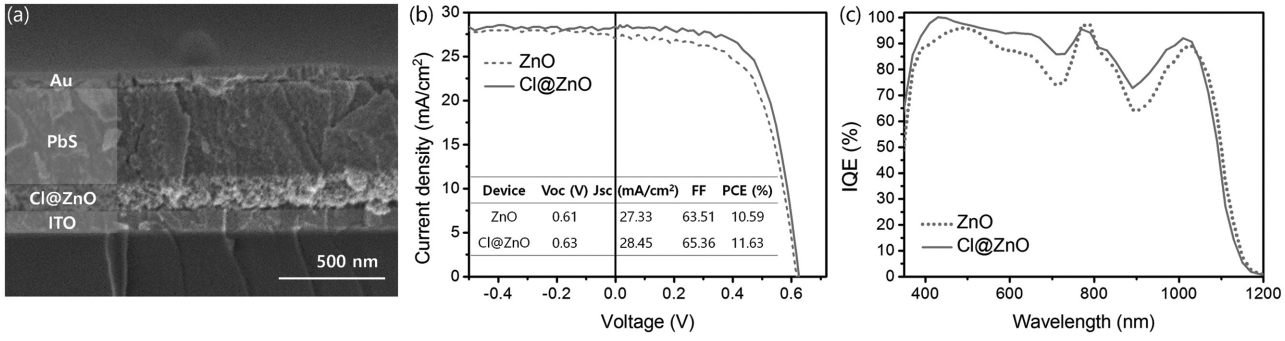

Figure 3. The effect of Cl@ZnO on CQD solar cell performance. a) Cross-sectional SEM image of a device consisting of ITO/Cl@ZnO/PbS/PbS–EDT/Au. b) Current density–voltage (*J–V*) characteristics of devices prepared using 1.32 eV bandgap PbS and c) internal quantum efficiency (IQE).

(10 mg mL^{-1} in methanol) was prepared with a 70 °C heat treatment for 10 min. The Cl@ZnO nanoparticle solution was prepared from mixing NaCl and ZnO solution (volume ratio of NaCl and ZnO solution is 1:4).

Synthesis of PbS CQDs: Lead halide-passivated PbS CQDs were produced by solution-phase ligand-exchange process with oleic-acid-capped CQDs (OA-CQDs) under air as described in previous report.[22] OA-CQDs were prepared using reported methods.[7] Solution of lead halides (0.1 M PbI_2 and 0.02 M $PbBr_2$) and NH_4Ac dissolved in dimethylformamide (DMF) was prepared for ligand exchange. 5 mL of OA-CQDs in octane (10 mg mL^{-1}) were mixed with the as-prepared DMF solution. For complete transfer of CQD toward DMF, 2 min vortexing was carried out at room temperature. The ligand-exchanged solution, where CQD are dispersed in DMF, was washed three times with octane for removing remained residues. After washing, toluene was added to the ligand exchanged solution for precipitation of CQD, and the CQDs were totally separated by centrifugation. Fully dried CQDs under vacuum for 20 min were redispersed in butylamine (BTA) with desired concentrations for film deposition.

Fabrication of Photovoltaics: The ITO glass was rinsed with detergent, distilled water, isopropyl alcohol, and acetone. As-prepared ZnO solutions were spin-coated on cleaned ITO glass at 3000 rpm for 30 s. The first PbS CQD layer was spin-coated onto ZnO substrate using as-prepared PbS CQDs in BTA with 2500 rpm for 30 s. After that, second EDT treated PbS layer was spin-coated on the first PbS CQD layer. For inducing PbS–EDT layer, OA-CQDs were deposited first, and then a 0.01 vol% EDT in acetonitrile (ACN) solution was coated on the OA-CQDs layer for 30 s, followed by three times ACN washing steps. For the top electrode, 120 nm Au was deposited on the PbS CQD film.

J–V Characterization: Photovoltaic performances of the devices were measured using Keithley 2400 source under AM 1.5G illumination of 100 mW cm^{-2} in N_2 atmosphere (Sciencetech class A). An aperture (active area 0.049 cm^2) was used for measurement. The spectral mismatch was calibrated by a reference solar cell (Newport).

EQE and IQE Measurements: EQE spectra were obtained from subjecting devices to monochromatic illumination (400 W Xe lamp passing through a monochromator and appropriate cutoff filters). The output power was corrected with Newport 818-UV and Newport 838-IR photodetectors. The beam was chopped at 220 Hz and focused in the pixel together with a solar-simulator at 1 sun intensity to provide for light bias. The beam was chopped at 220 Hz and focused in the pixel together with a solar-simulator at 1 sun intensity to provide for light bias. The IQEs of the PV devices using different ZnO layers were determined by EQE/[1 − $R(h\nu)$], where EQE is an external quantum efficiency, and $R(h\nu)$ is the reflectance at a photon energy of $h\nu$. R is derived from $A = 1 - R$, where A is double-pass absorption mode of the CQD devices, which are fully covered with Au metal electrode.

XPS and UPS Measurements: XPS and UPS spectra of ZnO films are measured on gold substrate. Photoelectron spectroscopy was carried out in a PHI5500 Multi-Technique system with monochromatic Al-K_α radiation (XPS) ($h\nu$ = 1486.7 eV) and nonmonochromatized He-I_α radiation (UPS) ($h\nu$ = 21.22 eV). Work functions (WF) were determined from the secondary electron cutoff (SEC) using equation WF = 21.22 eV—SEC. The differences between Fermi levels and valence band maximum were calculated from the low binding energy onset.

Other Measurements: Optical absorption measurements were obtained from a Lambda 950 500 UV–vis–IR spectrophotometer. Fielde-mission scanning electron microscopy (SEM) (Hitachi SU8230) was utilized for morphological and structural characterization. The capacitance–voltage measurements were acquired with an Agilent 4284A LCR meter at a frequency of 1 kHz and an AC signal of 50 mV, scanning from −1 to 1 V. All measurements were performed in the dark. The depletion width was calculated following previous reports.

Supporting Information

Supporting Information is available from the Wiley Online Library or from the author.

Acknowledgements

J.C., Y.K., and J.W.J. contributed equally to this work. The authors thank L. Levina, R. Wolowiec, D. Kopilovic, and E. Palmiano for their help over the course of this research. This research was supported by the Basic Science Research Program through the National Research Foundation of Korea (NRF) funded by the Ministry of Education (Nos. 2016R1A6A3A03009820 and 2016R1A6A3A03007170), and by the Ontario Research Fund Research Excellence Program, and by the Natural Sciences and Engineering Research Council (NSERC) of Canada.

Conflict of Interest

The authors declare no conflict of interest.

Keywords

band alignment, passivation, quantum-dot solar cells, ZnO

Received: April 26, 2017
Revised: May 28, 2017
Published online:

[1] V. M. Wood, J. Panzer, J. Chen, M. S. Bradley, J. E. Halpert, M. G. Bawendi, V. Bulović *Adv. Mater.* **2009**, *21*, 2151.
[2] K. Jeonghun, K. B. Wan, D. G. Lee, I. Park, J. Lim, M. Park, H. Cho, H. Woo, D. Y. Yoon, K. Char, S. Lee, C. Lee, *Nano Lett.* **2012**, *12*, 2362.
[3] X. Gong, Z. Yang, G. Walters, R. Comin, Z. Ning, E. Beauregard, V. Adinolfi, O. Voznyy, E. H. Sargent, *Nat. Photonics* **2016**, *10*, 253.
[4] G. Konstantatos, I. Howard, A. Fischer, S. Hoogland, J. Clifford, E. Klem, L. Levina, E. H. Sargent, *Nature* **2006**, *442*, 180.
[5] J.-S. Lee, M. V. Kovalenko, J. Huang, D. S. Chung, D. V. Talapin, *Nat. Nanotechnol.* **2011**, *6*, 348.
[6] A. H. Ip, S. M. Thon, S. Hoogland, O. Voznyy, D. Zhitomirsky, R. Debnath, L. Levina, L. R. Rollny, G. H. Carey, A. Fischer, K. W. Kemp, I. J. Kramer, Z. Ning, A. J. Labelle, K. W. Chou, A. Amassian, E. H. Sargent, *Nat. Nanotechnol.* **2012**, *7*, 577.
[7] Z. Ning, O. Voznyy, J. Pan, S. Hoogland, V. Adinolfi, J. Xu, M. Li, A. R. Kirmani, J. Sun, J. Minor, K. W. Kemp, H. Dong, L. Rollny, A. Labelle, G. Carey, B. Sutherland, I. Hill, A. Amassian, H. Liu, J. Tang, O. M. Bakr, E. H. Sargent, *Nat. Mater.* **2014**, *13*, 822.
[8] G.-H. Kim, F. P. García de Arquer, Y. J. Yoon, X. Lan, M. Liu, O. Voznyy, Z. Yang, F. Fan, A. H. Ip, P. Kanjanaboos, *Nano Lett.* **2015**, *15*, 7691.
[9] X. Lan, O. Voznyy, F. P. García de Arquer, M. Liu, J. Xu, A. H. Proppe, G. Walters, F. Fan, H. Tan, M. Liu, Z. Yang, S. Hoogland, E. H. Sargent, *Nano Lett.* **2016**, *16*, 4630.
[10] Y. Kim, K. Bicanic, H. Tan, O. Ouellette, B. R. Sutherland, F. P. García de Arquer, J. W. Jo, M. Liu, B. Sun, M. Liu, S. Hoogland, E. H. Sargent, *Nano Lett.* **2017**, *17*, 2349.
[11] C.-H. M. Chuang, P. R. Brown, V. Bulović, M. G. Bawendi, *Nat. Mater.* **2014**, *13*, 796.
[12] H. Aqoma, M. A. Mubarok, W. T. Hadmojo, E.-H. Lee, T.-W. Kim, T. K. Ahn, S.-H. Oh, S.-Y. Jang, *Adv. Mater.* **2017**, *29*, 1605756.
[13] S. A. McDonald, G. Konstantatos, S. Zhang, P. W. Cyr, E. J. D. Klem, L. Levina, E. H. Sargent, *Nat. Mater.* **2005**, *4*, 138.
[14] W. K. Bae, J. Joo, L. A. Padilha, J. Won, D. C. Lee, Q. Lin, W.-K. Koh, H. Luo, V. I. Klimov, J. M. Pietryga, *J. Am. Chem. Soc.* **2012**, *134*, 20160.
[15] F. Fan, O. Voznyy, R. P. Sabatini, K. T. Bicanic, M. M. Adachi, J. R. McBride, K. R. Reid, Y. S. Park, X. Li, A. Jain,

R. Quintero-Bermudez, M. Saravanapavanantham, M. Liu, M. Korkusinski, P. Hawrylak, V. I. Klimov, S. J. Rosenthal, S. Hoogland, E. H. Sargent, *Nature* **2017**, *544*, 75.
[16] A. G. Pattantyus-Abraham, I. J. Kramer, A. R. Barkhouse, X. H. Wang, G. Konstantatos, R. Debnath, L. Levina, I. Raabe, M. K. Nazeeruddin, M. Gratzel, E. H. Sargent, *ACS Nano* **2010**, *4*, 3374.
[17] J. Tang, H. Liu, D. Zhitomirsky, S. Hoogland, X. Wang, M. Furukawa, L. Levina, E. H. Sargent, *Nano Lett.* **2012**, *12*, 4889.
[18] G.-H. Kim, B. Walker, H.-B. Kim, J. Y. Kim, E. H. Sargent, J. Park, *Adv. Mater.* **2014**, *26*, 3321.
[19] A. J. Labelle, S. M. Thon, S. Masala, M. M. Adachi, H. Dong, M. Farahani, A. H. Ip, A. Fratalocchi, E. H. Sargent, *Nano Lett.* **2015**, *15*, 1101.
[20] G. H. Carey, L. Levina, R. Comin, O. Voznyy, E. H. Sargent, *Adv. Mater.* **2015**, *27*, 3325.
[21] X. Lan, O. Voznyy, A. Kiani, F. P. García de Arquer, A. S. Abbas, G. H. Kim, M. Liu, Z. Yang, G. Walters, J. Xu, M. Yuan, Z. Ning, F. Fan, P. Kanjanaboos, I. J. Kramer, D. Zhitomirsky, P. Lee, A. Perelgut, S. Hoogland, E. H. Sargent, *Adv. Mater.* **2016**, *28*, 299.
[22] M. Liu, O. Voznyy, R. Sabatini, F. P. Garcia de Arquer, R. Munir, A. H. Balawi, X. Lan, F. Fan, G. Walters, A. R. Kirmani, S. Hoogland, F. Laquai, A. Amassian, E. H. Sargent, *Nat. Mater.* **2017**, *16*, 258.
[23] H. Liu, J. Tang, I. J. Kramer, R. Debnath, G. I. Koleilat, X. H. Wang, A. Fisher, R. Li, L. Brzozowski, L. Levina, E. H. Sargent, *Adv. Mater.* **2011**, *23*, 3832.
[24] J. B. Gao, C. L. Perkins, J. M. Luther, M. C. Hanna, H. Y. Chen, O. E. Semonin, A. J. Nozik, R. J. Ellingson, M. C. Beard, *Nano Lett.* **2011**, *11*, 3263.
[25] J. Jean, S. Chang, P. R. Brown, J. J. Cheng, P. H. Rekemeyer, M. G. Bawendi, S. Gradecak, V. Bulović, *Adv. Mater.* **2013**, *25*, 2790.
[26] P. H. Rekemeyer, S. Chang, C.-H. M. Chuang, G. W. Hwang, M. G. Bawendi, S. Gradečak, *Adv. Energy Mater.* **2016**, *6*, 1600848.
[27] R. Azmi, H. Aqoma, W. T. Hadmojo, J. M. Yun, S. Yoon, K. Kim, Y. R. Do, S. H. Oh, S. Y. Jang, *Adv. Energy Mater.* **2016**, *6*, 1502146.
[28] M. Liu, P. F. de Arquer, Y. Li, X. Lan, G. H. Kim, O. Voznyy, L. Jagadamma, A. Abbas, S. Hoogland, Z. Lu, J. Kim, A. Amassian, E. H. Sargent, *Adv. Mater.* **2016**, *28*, 4142.
[29] R. L. Z. Hoye, B. Ehrler, M. L. Bohm, D. Munoz-Rojas, R. M. Altamimi, A. Y. Alyamani, Y. Vaynzof, A. Sadhanala, G. Ercolano, N. C. Greenham, R. H. Friend, J. L. MacManus-Driscoll, K. P. Musselman, *Adv. Energy Mater.* **2014**, *4*, 1301544.
[30] L. K. Jagadamma, M. Abdelsamie, A. E. Labban, E. Aresu, G. O. Ngongang Ndjawa, D. H. Anjum, D. Cha, P. M. Beaujuge, A. Amassian, *J. Mater. Chem. A* **2014**, *2*, 13321.
[31] J. B. Baxter, C. A. Schmuttenmaer, *J. Phys. Chem. B* **2006**, *110*, 25229.
[32] S. Y. Shao, K. B. Zheng, T. Pullerits, F. L. Zhang, *ACS Appl. Mater. Interfaces* **2013**, *5*, 380.
[33] G. Yang, H. Tao, P. Qin, W. Kea, G. Fang, *J. Mater. Chem. A* **2016**, *4*, 3970.
[34] P. R. Brown, D. Kim, R. R. Lunt, N. Zhao, M. G. Bawendi, J. C. Grossman, V. Bulović, *ACS Nano* **2014**, *8*, 5863.
[35] J. P. Correa Baena, L. Steier, W. Tress, M. Saliba, S. Neutzner, T. Matsui, F. Giordano, T. J. Jacobsson, A. R. Srimath Kandada, S. M. Zakeeruddin, A. Petrozza, A. Abate, M. K. Nazeeruddin, M. Grätzel, A. Hagfeldt, *Energy Environ. Sci.* **2015**, *8*, 2928.
[36] J. Choi, S. Song, M. T. Hörantner, H. J. Snaith, T. Park, *ACS Nano* **2016**, *10*, 6029.
[37] I. Robel, M. Kuno, P. V. Kamat, *J. Am. Chem. Soc.* **2007**, *129*, 4136.
[38] B. Ehrler, K. P. Musselman, M. L. Böhm, F. S. F. Morgenstern, Y. Vaynzof, B. J. Walker, J. L. MacManus-Driscoll, N. C. Greenham, *ACS Nano* **2013**, *7*, 4210.
[39] Y. E. Ha, M. Y. Jo, J. Park, Y.-C. Kang, S. I. Yoo, J. H. Kim, *J. Phys. Chem. C* **2013**, *117*, 2646.
[40] S. B. Jo, J. H. Lee, M. Sim, M. Kim, J. H. Park, Y. S. Choi, Y. Kim, S.-G. Ihn, K. Cho, *Adv. Energy Mater.* **2011**, *1*, 690.
[41] S. Bai, Y. Jin, X. Liang, Z. Ye, Z. Wu, B. Sun, Z. Ma, Z. Tang, J. Wang, U. Würfel, F. Gao, F. Zhang, *Adv. Energy Mater.* **2015**, *5*, 1401606.
[42] V. Ischenko, S. Polarz, D. Grote, V. Stavarache, K. Fink, M. Driess, *Adv. Funct. Mater.* **2005**, *15*, 1945.
[43] J. B. Cui, Y. C. Soo, T. P. Chen, U. J. Gibson, *J. Phys. Chem. C* **2008**, *112*, 4475.
[44] F. Wang, J.-H. Seo, Z. Li, A. V. Kvit, Z. Ma, X. Wang, *ACS Appl. Mater. Interfaces* **2014**, *6*, 1288.
[45] J. C. Klein, D. M. Hercules, *J. Catal.* **1983**, *82*, 424.
[46] V. I. Nefedov, Y. V. Salyin, G. Leonhardt, R. Scheibe, *J. Electron Spectrosc. Relat. Phenom.* **1977**, *10*, 121.
[47] S. Olthof, S. Mehraeen, S. K. Mohapatra, S. Barlow, V. Coropceanu, J.-L. Brédas, S. R. Marder, A. Kahn, *Phys. Rev. Lett.* **2012**, *109*, 176601.
[48] H. Tan, A. Jain, O. Voznyy, X. Lan, F. P. Garcia de Arquer, J. Z. Fan, R. Quintero-Bermudez, M. Yuan, B. Zhang, Y. Zhao, F. Fan, P. Li, L. N. Quan, Y. Zhao, Z.-H. Lu, Z. Yang, S. Hoogland, E. H. Sargent, *Science* **2017**, *355*, 722.

